Nanosized silver, but not titanium dioxide or zinc oxide, enhances oxidative stress and inflammatory response by inducing 5-HETE activation in THP-1 cells

Wing-Lam Poon,[1]* Jetty Chung-Yung Lee,[1]* Kin Sum Leung[1], Harri Alenius,[2,3] Hani El-Nezami,[1,4§] Piia Karisola[2§]

[1]School of Biological Sciences, University of Hong Kong, Pokfulam Road, Hong Kong
[2]Human Microbiome Research Program, University of Helsinki, Haartmaninkatu 3, 00290 Helsinki, Finland
[3]Institute of Environmental Medicine (IMM), Karolinska Institutet, Stockholm 171 77, Sweden
[4]Nutrition and health, Institute of Public Health and Clinical Nutrition, University of Eastern Finland, P.O. Box 1627, 70211 Kuopio, Finland

*These authors contributed equally to this work.
[§]Address correspondence to piia.karisola@helsinki.fi and elnezami@hku.hk

Author's contact information:
BSc Wing-Lam Poon, Tel. (852) 2299 0834, vpoon11@connect.hku.hk
Assist. Prof. Jetty Chung-Yung Lee, Tel. (852) 2299 0318, jettylee@hku.hk
PhD Dr Kin Sum Leung, Tel. (852) 2299 0834, sam612@connect.hku.hk
Prof. Harri Alenius, Tel. (358) 2941 26460, harri.alenius@helsinki.fi
Prof. Hani S. El-Nezam, Tel. (852) 2299 0835, elnezami@hku.hk
Assoc. Prof. Piia Karisola, Tel. (358) 2941 26601, piia.karisola@helsinki.fi

Word count: 6073

Keywords:
Nanoparticles; metal oxides; fatty acid metabolism; glutathione (GST); superoxide dismutase (SOD); monocyte; LC/MS; ICP/MS; microarray analysis; inflammation; chemotaxis.

Abstract

Bioactive, oxygenated metabolites of polyunsaturated fatty acids (PUFAs) are important indicators of inflammation and oxidative stress but almost nothing is known about their interactions with nanomaterials (NMs). To investigate the effects of nano-sized materials (n-TiO_2, n-ZnO, n-Ag) and their bulk-sized or ionic (b-TiO_2, b-ZnO, i-Ag) counterpart, we studied the status of oxidative stress and PUFA metabolism in THP-1 cells at low-toxic concentrations (<15% cytotoxicity) 6 h or 24 h after the particle exposures by LC/MS and microarray. N-Ag had a significant and sustained impact on cellular antioxidant defense, seen as incremental synthesis and accumulation of glutathione (GSH) in the cell, and reduction of superoxide dismutase (SOD) activity. The cellular particle doses were largely dependent on exposure duration and particle dissolution, and active transporter mechanisms controlled the concentration of Zn in cytosol. Even at these sub-toxic concentrations, n-Ag was able to induce statistically significant elevation in the 5-HETE : arachidonic acid ratio at 24 h, which suggests association to oxidative stress and induction of pro-inflammatory responses. This was supported by the enhanced gene expression of chemotaxis-related genes. Overall, THP-1 cells internalized all tested particles, but only n-Ag led to low level of oxidative stress through ROS production and antioxidant balance disruption. N-Ag stimulated arachidonic acid oxidation to form 5-HETE which further magnified the inflammatory responses by enhancing the production of mitochondrial superoxide and leukocyte chemokines. Since the sustained n-Ag uptake was detected, the effects may last long and function as a trigger for the low-grade inflammation playing role in the chronic inflammatory diseases.

Introduction

Metal-based nanoparticles (metals and metal oxides) are widely used engineered nanomaterials (NM), in particular, nano-sized titanium dioxide (n-TiO_2) and zinc oxide (n-ZnO) are the most produced NM globally on a mass basis, and silver nanoparticles (n-Ag) are the most frequently used NM in consumer products (Vance et al. 2015). Together, they comprise 48% of the consumer products with known nanomaterial compositions registered in the nanodatabase (DTU Environment). In addition to their new and beneficial characteristics, NMs have raised health concerns due to the small size that possibly permits easier access to body and cellular targets which are otherwise unreachable by their chemically identical but physically larger counterparts (Kreyling et al. 2009, Pietroiusti et al. 2013, Pietroiusti et al. 2018). The signature of small size also means greatly increased surface reactivity and potentially higher toxicity (Sharifi et al. 2012). Depending on other physicochemical properties such as shape, surface chemistry, dissolution, and aggregation, different mechanisms may be involved in the toxicity of NMs. Induction of inflammation and oxidative stress are often reported (Fu et al. 2014, Khanna et al. 2015, Palomaki et al. 2011, Pietroiusti et al. 2018), and they were also observed in our previous transcriptomic study (Poon et al. 2017).

Polyunsaturated fatty acids (PUFAs) are important constituents in all eukaryotes, they are responsible for the structural integrity of biological membranes (Durand et al. 2011) and generate a variety of lipid signalling molecules, namely eicosanoids (derived from arachidonic acids, AA and eicosapentaenoic acid, EPA) and docosanoids (derived from docosahexaenoic acid, DHA) (Dennis and Norris 2015). These bioactive oxygenated PUFA metabolites are important indicators of inflammation and oxidative stress (Huang et al. 2014), and are highly relevant in numerous pathophysiological processes (Funk 2001, Yin et al. 2013). Under inflammation, PUFAs can be oxidized enzymatically by lipoxygenases (LOXs), cyclooxygenases (COXs), or by cytochrome (CYP) P450s to hydroxyeicosatetraenoic acids (HETEs), prostaglandins and hydroxydocosahexaenoic acids (HDoHEs) (Dennis and Norris 2015). Under oxidative stress, PUFAs can be oxidized non-enzymatically by free radicals to other bioactive lipids, among which isoprostanes (IsoPs) represent a group of important biomarkers for oxidative stress in mice (Qin 2012) and humans (Durand et al. 2011). Together, these oxidized lipids make up an important signalling network of the innate immune response, with both pro-inflammatory and anti-inflammatory functions depending on the lipid profile (Dennis and Norris 2015). Therefore, their characterization is highly relevant also in the study of NM toxicity.

Currently, research on interactions between NMs and PUFA metabolism is very scarce. Only a recent study shows that exposure to TiO_2 nanoparticles (10 nm, anatase) causes increased production of several COX-2 metabolites in mouse macrophage cell lines (Chen et al. 2018), but no one has explored PUFA/eicosanoid metabolism by lipidomic profiling. In this study, we investigated the effects of Ag, ZnO and TiO_2 nanoparticles (n-Ag, n-TiO_2, n-ZnO) on the oxidative stress status and PUFA metabolism in differentiated THP-1 cells. Since tissue macrophages are the first and important immune cells to encounter and engulf NMs in exposed gut, skin and lungs, we simulated these natural

interactions by differentiating THP-1 cells to exhibit a macrophage-like phenotype including enhanced adherence and phagocytosis abilities (Qin, 2012). These maturated THP-1 cells are able to express and secrete several chemokines, which in a living organism would recruit neutrophils, monocytes and lymphocytes to resolve the NM-originated danger. Integrating with the transcriptomic data, we showed that n-Ag triggered the most severe inflammation among all tested nanoparticles, which involved the exclusive production of 5-HETE from AA oxidation accompanying the enhanced transcription of a set of chemokines. Mitochondrial superoxide production, reduced superoxide dismutase activity and GSH accumulation were also detected with n-Ag exposure, indicating oxidative stress in the cell.

Materials and methods

Particles

Nano-sized titanium dioxide (n-TiO_2, 90% of rutile and 10% of anatase) and zinc oxide (n-ZnO) were purchased from Nanostructured & Amorphous Materials, Inc. (Houston, USA). Nano-sized PVP-coated silver (n-Ag) was purchased from NanoComposix (San Diego, USA), bulk-sized titanium dioxide (b-TiO_2) from Sigma-Aldrich (Schnelldorff, Germany), bulk-sized zinc oxide (b-ZnO) from Camden-Grey Essential Oils, Inc. (Doral, USA), and silver nitrate ($AgNO_3$) from Sigma-Aldrich (USA). Properties of n-TiO_2, b-TiO_2, n-ZnO, b-ZnO and n-Ag provided by the vendors are shown in Poon et al. (2017). These particles were characterized in (Poon et al. 2017).

Particle dispersions

The n-TiO_2, b-TiO_2, n-ZnO and b-ZnO particles were weighed into autoclaved glass tubes. Stock dispersions (1 mg/ml) were prepared in complete media (cRPMI) followed by 20 min sonication at 30 °C (Elmasonic S15H, Tovatech LLC South Orange, NJ, USA). Final dispersions were prepared from serial dilution of the stock in cRPMI followed by another 20 min sonication at 30 °C just before the cell experiment. The aqueous stock solution of n-Ag was a 1 mg/ml, and before use, it was shaken vigorously for 30 s to ensure homogeneity. Silver ion solution (i-Ag), $AgNO_3$, was dissolved in Milli-Q water to form a 0.3 % stock solution and sterile filtered. Final dispersions were prepared by dilution in complete media. All dispersions were vortexed for 10 s after sonication, 5 s during serial dilutions and before dosing the cells.

Cell exposures

A human monocytic cell line, THP-1 cells (ATCC, Rockville, MD, USA) were grown in RPMI (Gibco, Life Technologies, Grand Island, NY, USA) supplemented with 10 % fetal bovine serum (Gibco), 1 % GlutaMAX (Gibco), 1 % HEPES (Gibco), 0.05 mM 2-ME (Sigma-Aldrich, Schnelldoff, Germany), and 1 % PEST (Gibco) at 37 °C with a humidified atmosphere of 5 % CO_2. Cells were seeded into each 35 x 10 mm dish (growth area: 11.78 cm^2) at a density of 0.9 x 10^6 cells/ml in 2.48 of medium. At all study setups, THP-1 cells were differentiated to macrophage-like phenotype in cRPMI containing 50 nM phorbol-12-myristate-13-acetate (PMA, Cat. P8139, Gibco) for 48 h in total. After first 24 h, the medium was replaced with freshly prepared differentiation medium, half of the original volume, for the next 24 h. Based on the previous analyses, all the experiments were carried out at the concentration of nanomaterials, which corresponds to minimum of 85 % cell viability. The differentiated cells were treated with 100 μg/ml n/b-TiO_2, 10 μg/ml n/b-ZnO or n-Ag, or 1 μg/ml i-Ag for 6 h or 24 h.

Afterwards, cells were rinsed with PBS twice and then scrapped off from the dish in 520 µl PBS containing 1 mM EDTA and 0.1 % triton X-100 for 6 h samples and 200 µl for 24 h samples. Collected cell suspension was vortexed briefly (~5 s) and bath sonicated at 4 °C for 1 min to lyse the cells. 200 µl (6 h) or 50 µl (24 h) of the cell lysate was aliquoted and centrifuged at 1,500 x g, at 4 °C for 5 min, and the supernatant was stored at -80 °C for the SOD activity assay. The remaining cell lysate was centrifuged at 10,000 x g at 4 °C for 15 min. 100 µl (6 h) or 30 µl (24 h) of the supernatant was aliquoted and stored at -80 °C for protein quantification. 200 µl (6 h) or 110 µl (24 h) of the remaining supernatant was transferred to a new microcentrifuge tube, and mixed with an equal volume of freshly prepared metaphosphoric acid (0.1 g/ml, Sigma-Aldrich 239275). After incubation of 5 min at room temperature (RT), the mixture was centrifuged at >2,000 x g for 2 min. The supernatant was collected and stored at -20 °C for the GSH assay. These additional steps before sample storage was to deproteinize the samples and minimize the interference due to any sulfhydryl groups on proteins from the sample during assaying for the GSH content.

For the LC-MS/MS experiment, cells were grown into 60 x 15 mm dish (growth area: 21.5 cm^2) at a density of 0.9 x 10^6 cells/ml in 4.5 ml of medium. After particle exposures, cells were rinsed twice with PBS and then scrapped off from the dish in 1.13 ml of PBS mixed with 20 µl 2 mM butylated hydroxytoluene (BHT) in ethanol and 20 µl 5 mM indomethacin in ethanol, and collected into 15-ml Falcon tubes. A volume of 100 µl cell suspension was aliquoted for protein quantification, and mixed with 100 µl of RIPA buffer containing 1% protease inhibitor cocktail (Sigma-Aldrich, US, P8340). All samples were stored at -80 °C before further analysis.

DC protein assay and sample dilutions

To quantify the protein content in the samples for normalization, DC protein assay (Bio-Rad, Cat. 500-0111, US) was performed following the microplate plate assay protocol on the manufacturer's manual. In brief, 5 µl of diluted samples or BSA standards was mixed with 25 µl of reagent A' (an alkaline copper tartrate solution) and 200 µl of reagent B (a dilute Folin reagent) on a 96-well microplate to allow the reaction to occur. After 15 min of incubation at RT, absorbance was read at 750 nm. The protein concentrations of samples were calculated from the standard curve that covered from 0.03125 mg/ml to 2 mg/ml of BSA.

For sample dilution, undiluted samples were used to normalize for the SOD and GSH assays, whereas 2-fold diluted samples were used to normalize for the LC-MS lipid quantification.

Total glutathione (GSH) assay

Total glutathione content in the cells was measured by Cayman Glutathione Assay Kit (Item 703002, USA), which measures both the reduced form (GSH) and the oxidized form (GSSG) of GSH. All steps were performed following the manufacturer's instructions. In brief, the deproteinated samples were thawed on ice and mixed with a freshly prepared 4M solution of triethanolamine (Sigma-Aldrich,

Cat. T58300) to increase their pH for assaying. The 6 h and 24 h samples were then diluted in MES buffer for 2 folds and 4 folds respectively. 50 µl of diluted samples or GSSG standards were mixed with 150 µl of freshly prepared Assay cocktail on 96-well plate and incubated at RT for 25 min. The absorbance was read at 410 nm, and the total GSH content was calculated from the standard curve and normalized with the protein content.

Superoxide dismutase (SOD) activity assay

Cytosolic and mitochondrial SOD was measured by Cayman Superoxide Dismutase Assay Kit (Item 706002, USA), which detects activity of all three types of SODs related to Cu/Zn, Mn, and FeSOD. All steps were performed following the manufacturer's instructions. In brief, the 6 h and 24 h samples were diluted for 5 and 10 folds respectively and assayed in duplicates. 10 µl of the diluted samples or SOD standards were mixed with 200 µl of diluted radical detector (a tetrazolium salt solution) and 20 µl of diluted xanthine oxidase on a 96-well plate. The reaction mixture was incubated at RT for 30 min before absorbance was measured at 450 nm. The SOD activity was calculated from the standard curve, normalized with the protein content and expressed as U/mg protein, where one unit of SOD was defined as the quantity of enzyme required for 50 % dismutation of the superoxide.

Measurement of mitochondrial superoxide production

Cells were seeded and differentiated on 96-well plate at a density of 0.9 x 10^6 cells/ml for 48 h. After particle exposures, cells were rinsed with PBS twice, and incubated with 34 µl of 5 µM MitoSOX Red (Molecular Probes, Thermo Fisher Scientific, Waltham, MA, USA) working solution in the dark (cell incubator) at 37 °C for 10 min. The reagent was then discarded and cells were gently washed twice with PBS. Images of live cells were taken using a confocal laser scanning microscope (Carl Zeiss LSM 710 NLO) and the fluorescence intensity was quantified using Image J software (nih.gov).

Cellular particle dose and particle dissolution quantification by inductively coupled plasma mass spectrometry (ICP-MS)

For the ICP-MS experiment, the cells were seeded on 24-well plate at a density of 0.9 x 10^6 cells/ml in 400 µl of medium, differentiated for 48 h. After particle exposures, the cells were rinsed with PBS three times before acid digestion. For control and n/b-ZnO and n/i-Ag samples, the cells were digested in 100 µl of concentrated nitric acid (~ 70 %) overnight at dark. Digested samples were 7-fold diluted with MQ water and then stored as stock at 4 °C in the dark before the ICP-MS analysis. For n/b-TiO_2 samples, the cells were incubated with 1.1 ml of a mix of hydrofluoric acid (HF) and concentrated nitric acid (HNO_3) on a 70 °C hot water bath for 2 h to complete the digestion. The HF/HNO_3 acid mix was prepared from a 48 % HF stock mixing with a concentrated HNO_3 stock (~ 70 %) and MQ

water in a ratio of 4:4:3. After digestion, the TiO_2 samples were stored as stock at 4 °C in the dark before the ICP-MS analysis.

To evaluate the particle dissolution, the same particle dispersions used for cell treatment was incubated at the same condition as the cells during the 24 h exposure period. Afterwards, 100 µl of supernatant containing the released ions, i.e. the released fraction, was collected after two centrifugation steps at 20,800 x g at 4 °C (first for 10 min, second for 50 min). Like the cell samples, for n/b-ZnO and n-Ag samples, 100 µl of concentrated HNO_3 was added to digest the samples overnight at dark. The samples were then diluted with 500 µl of MQ water and stored as stock at 48 °C in the dark before the ICP-MS analysis. For the n/b-TiO_2 samples, the collected supernatants were digested in 1 ml of HF/HNO_3 acid mix (HF : HNO_3 : H_2O = 2 : 2 : 1) on the 70 °C hot water bath for 2 h. They were stored at 4 °C in the dark before ICP-MS analysis. Just before the analysis, the samples were further diluted to achieve the final dilutions, which were 2% HNO_3 for ZnO and Ag samples and 2.545 % HNO_3/1.745 % HF for TiO_2 samples. Three measurements were made by the ICP-MS for each sample.

Gene expression

Gene expression arrays were performed as in (Poon et al. 2017). Shortly after the differentiated THP-1 cells were exposed to different particles for 6 h or 24 h, total RNA was extracted and transcriptomics was studied in the gene expression arrays (Agilent technologies; Sure Print G3 Human GE v3 8x60K, USA).

Extraction of PUFA oxidation products

PUFA oxidation products were extracted from cell samples (~4×10^6 cells) according to Dupuy et al. method (Dupuy et al. 2016). In brief, cell samples in 15-ml Falcon tubes were freeze – thawed, and homogenized in 10 ml of Folch solution (chloroform/methanol, 2:1 vol/vol + 0.05% BHT) on ice using blade homogenizer (T25, ULTRA-TURRAX, IKA). After shaking with orbital shaker on ice for 30 min, phase separation was introduced by adding 2 ml of 0.9 % NaCl. Then, the mixture was shaken on ice for 30 min and centrifuged at 2000 × g for 10 min at RT. The lower chloroform phase was collected in a 30 ml glass vial. 5 ml of chloroform was added to the 15-ml Falcon tube. After another 5 min centrifugation at RT, the lower phase was collected to the same 30 ml glass vial to recover as much extract as possible. The collected sample extracts were dried completely on 37 °C heating block under a stream of nitrogen. 1 ml of potassium hydroxide (1 M) in methanol, together with 1 ml of PBS were added to the cell extract to perform alkaline hydrolysis overnight at RT. To stop the alkaline hydrolysis, 200 µl of 5 N hydrochloric acid, 0.5 ml of methanol, 2.7 ml of 40 mM formic acid and 4 ml of 20 mM formic acid was added to the extracts. Afterwards, the sample extracts were cleaned using mixed anion solid phase extraction (SPE, MAX Waters, USA). As follows, the SPE column was preconditioned with methanol and 20 mM formic acid. After loading the sample, 2

% ammonium hydroxide and 20 mM formic acid were used for washing the impurities. The purified extract was collected with 6 ml hexane : ethanol : acetic acid (70 : 29.4 : 0.6 volumes). The samples were then dried at 37 °C under a stream of nitrogen gas until complete dryness. The dried extracts were re-suspended in 100 µl of an internal standard mix (0.1 ng/µl in methanol), then filtered by 0.45 µm polytetrafluoroethylene membrane filter to remove insoluble impurities and immediately analyzed by LC-MS/MS.

Measurement of PUFA oxidation products by liquid chromatography tandem mass spectrometry (LC-MS/MS)

The Sciex X500R QTOF system (Sciex Applied Biosystems, MA, USA) consisted of an Exion LC AC liquid chromatograph with a C18 column (150 x 2.1 mm, 2.6 µm particle size, Phenomenex, USA) was maintained at 40 °C for analysis. The flow rate was set to 300 µl / min and the injection volume was 10 µl. The mobile phase consisted of 0.1 % aqueous acetic acid in water (A) and 0.1% acetic acid in methanol (B). The gradient was first maintained at 20 % of solvent B for 2 min and then increased to 98 % in 8 min. 98% of B was held for 5 more min. Finally, the percentage of solvent B was reduced to 20 % in 1 min and held for an additional 5 min to equilibrate to the initial condition. The X500R QTOF system was operated in negative electrospray ionization (ESI) mode. The spray voltage was set to -4500 V and nitrogen was the curtain gas. The ionization chamber temperature was set at 350 °C, and the pressure of the ion source gas 1 and 2 were set at 35 and 45 psi, respectively. In the TOF MS, the declustering potential (DP) was set to -80 V and the collision energy (CE) was -10 V. The scan mode was multiple reaction monitoring (MRM). All data collected by the X500R QTOF system was analyzed by the Sciex operating system (version 1.2.0.4122). All standards (PUFA, HETE, HDoHE, resolvins, F_2-Isoprostanes) were purchased from Cayman Chemicals (USA) and a total of 17 oxidized PUFA products were measured. The quantification of each analyte was determined by correlating the peak area to its corresponding deuterated internal standard peak. For the analytes without its corresponding deuterated internal standards, quantitation was made by using deuterated internal standards with similar structures i.e. 5(S)-HETE-d_8 was used for 8(S)-, 9(S)- and 11(S)-HETE, DHA-d_5 for resolvin RvD1 and all HDoHEs, and EPA-d_5 for resolvin RvE1.

Results

N-Ag disrupts cellular antioxidant defense and ROS production

The level of total glutathione (GSH, both oxidized and reduced forms) was quantified by the color-generating reaction between glutathione and DTNB (5,5′-Dithiobis(2-nitrobenzoic acid)) in the cells after the NM exposure. N-Ag yielded significant increase of total GSH at 24 h when compared to unexposed controls (Fig. 1A). Other tested particles (ZnO and TiO_2) did not cause any changes except b-ZnO, which significantly increased the level of total glutathione at 6 h, but the effect was resolved already at 24 h (Fig. 1A). These results were supported by the increased expression of the GCLC gene in the microarray study (Fig. 1B). GCLC encodes the catalytic subunit of glutamate-cysteine ligase (GCL), catalyzing the first rate-limiting step in glutathione synthesis.

Activity of antioxidant superoxide dismutase (SOD), found in cytosol and mitochondrion, was significantly inhibited by i-Ag at both time points and by n-Ag at 24 h (Fig. 1C). However, confocal microscopy imaging with MitoSOX Red dye, which permeate to live cells and gets selectively oxidized by mitochondrial superoxide, showed that only n-Ag triggered mitochondrial superoxide production at the same time point (Fig. 1D). SOD2, the primary antioxidant enzyme that scavenges superoxide radicals in mitochondria, was highly upregulated with all ZnO and Ag particles at both time points (Fig. 1E).

Cellular particle dose changes over time and is related to particle solubility

The cellular particle dose, which includes internalized particles, released ions and particles firmly attached to the cell membrane, was measured by ICP-MS. Exposure to all three NMs resulted in different cellular dose compared to their bulk-sized or ionic material at 24 h (Fig. 2A-C). While the difference in the cellular Ti concentrations was small at 24 h (Fig. 2A), the cellular Zn concentration in b-ZnO-treated cells was about one-third greater when compared to cells treated by the n-ZnO at 24 h (Fig. 2B). The cellular concentration of Ag was over 100 times greater in n-Ag-treated cells compared to i-Ag-treated cells (Fig. 2C). The gene expression changes were also studied by transcriptomics. The n-/b-ZnO and n-Ag caused changes in the expression of zinc transporters at both 6 h and at 24 h (Fig. 2D-E). All particles reduced the expression of a Zn ion importer gene, ZIP10 (Fig. 2D), and increased the expression of two Zn ion exporter genes, ZnT1 and ZnT2 (Fig. 2E).

The cellular dose usually increased along with time as seen with the TiO_2 and Ag particles (Fig. 2A, C), but for ZnO particles, the cellular concentrations decreased over time (Fig. 2B). Percentage of dissolution (% dissolution) of all particles in culture medium after 24 h incubation was measured by ICP-MS quantification of released ions in the supernatant (Table 1). ZnO particles were found to be the most soluble with 51.9% and 58.4% of dissolution for n-ZnO and b-ZnO, respectively. N-Ag was almost insoluble with only 1.7% dissolution recorded. TiO_2 particles were insoluble within the detection limit. When the absolute cellular dose is converted into percentage of total particles added,

the cellular uptake of particles with low solubility, especially TiO_2 and n-Ag, was much higher than with the more soluble ZnO particles and silver nitrate (i-Ag) (Table 1).

Induction of 5-HETE production by n-Ag

To investigate whether the three metal-based NMs caused enzymatic oxidation of PUFAs, the levels of different enzymatic oxidation metabolites of PUFA and the precursor PUFA were measured by LC-MS/MS. The concentrations of PUFA were not significantly changed by the NMs after 6 h and 24 h exposure (Table S1).

The results of the oxidized PUFA products were expressed as a ratio of the products versus the respective precursor. Isomers of LOX-mediated HETEs (5-, 12- and 15-HETE) and HDoHEs (4-, 7-, 8-, 11-, 14- and 17-HDoHE), and CYP-mediated HETEs (8-, 9-, 11- and 20-HETE) were detected (Fig. 3A). However, COX-mediated $PGF_{2\alpha}$, RvD1 and RvE1 were below the limit of detection (<1 pg) and therefore were not quantitated.

Notably, the ratio of 5-HETE to AA was significantly increased by n-Ag at 24 h (Fig. 3B). No statistically significant changes in other HETEs (12- and 15-HETE) and HDoHEs (4-, 7-, 8-, 11-, 14- and 17-HDoHE) were observed in cells exposed to i-Ag, TiO_2 or ZnO particles for 24 h compared to the control group (Table S1 and Fig. S1). The HETEs and HDoHEs were not altered by the NM exposure after 6 h.

In addition, to confirm that the NMs did not participate in non-enzymatic oxidative stress, the novel oxidative stress biomarker, F_2-Isoprostanes (F_2-IsoPs) derived from AA was measured. There were no changes in the ratio when compared to the control group after 6 h and 24 h exposures (Fig. 3C, Table S1).

PUFA metabolism and chemotaxis by gene expression

Gene expression of several enzymes involved in oxidation of PUFA were also found to be disrupted by n-Ag in the microarray analyses especially at 24 h. Phospholipase A2 isozymes are responsible for the hydrolytic release of sn-2 fatty acid (including AA) from membrane phospholipids and some of them were upregulated (PLA2G4C) by n/b-ZnO and especially by n-Ag, when compared to unexposed controls (Fig. 4A). ALOX5 (5-LOX, Fig. 4B), which catalyzes the conversion of AA to 5-HpETE (the precursor of 5-HETE), and its activating protein, ALOX5AP (FLAP, Fig. 4C) were down-regulated, whereas expression of the COX-2 gene (called also PTGS2) was found to be increased exclusively by n-Ag (Fig. 4D).

The gene expression of several chemokines, which play a role in recruiting cells to the target site was studied. CCL3 (MIP1α), CXCL2 (MIP2α) and CXCL1 (NAP-3), which are all neutrophil attracting chemokines were upregulated mainly by n/b-ZnO and to a larger extent by n-Ag at both

time points (Fig. 5A). Also, chemotaxis for monocytes and T cells was induced by expression of CXCL3 (MIP2β) and CCL17 (TARC), respectively (Fig. 5B).

Discussion

Oxidative stress is a condition of redox imbalance in the cell. This is caused by the over-production of reactive oxygen species (ROS) that exceeds the capacity of cellular antioxidant defense (Sies 1985). It is one of the most widely proposed mechanisms of NM toxicity, involving three stages of action. Low level of nanoparticle-induced oxidative stress enhances *nrf*2-mediated transcription of antioxidant defense genes. Moderate oxidative stress causes activation of NFκB-mediated signaling for inflammation. Furthermore, a very high level of oxidative stress activates apoptotic and necrotic pathways (Nel et al. 2006, Sharifi et al. 2012). To understand the overall oxidative stress status of differentiated THP-1 cells upon exposure to the selected nanoparticles, effects on several representative cellular antioxidants (GSH and SOD), the major source of cellular ROS (mitochondrial superoxide) and oxidative stress markers were investigated in the current study.

GSH is the largest source of low-molecular-weight thiol (R-SH), and its oxidized and reduced forms compose the major redox pair in animal cells, playing an important role in anti-oxidant defense (Wu et al. 2004). The thiol group offers an additional protection against metal stress as it can chelate reactive, free metal ions (Hernandez et al. 2015, Leung et al. 2013), and facilitate their excretion from the cell (Ballatori et al. 2009). GSH synthesis is largely dependent on the activity of its first rate-limiting step enzyme, glutamate-cysteine ligase (GCL), and is encoded by the two genes: GCLC (catalytic subunit) and GCLM (modifier subunit). Induction of this enzyme can be triggered at least by oxidant stress, inflammatory cytokines and heavy metals (Wu et al. 2004). In our current work, we found that cellular GSH in THP-1-differentiated macrophages was significantly increased by n-Ag with an elevated GCLC gene expression, implying incremental GSH synthesis and its subsequent accumulation in the cells during the 24 h of exposure. This is thought to be a response to defend against the increasing ROS production and/or the released toxic metal ions by the cell (Xu et al. 2014). These data are in line with many studies that show altered cellular GSH level together with the ROS production triggered by Ag NMs as reviewed by Cameron et al (Cameron et al. 2018).

Superoxide dismutase (SOD) is another important cellular antioxidant. While the level of GSH is more associated with the general redox status in the cell, SOD specifically converts superoxide (O_2^-) into oxygen (O_2) and hydrogen peroxide (H_2O_2) (Fukai and Ushio-Fukai 2011). Ag ion, however, can bind SOD at the copper-binding sites, inhibiting its enzymatic activity (Ciriolo et al. 1994). Such reduction in SOD activity impairs the capacity for superoxide neutralization and may lead to accumulation of the ROS species. In the current study, we showed that both n-Ag and i-Ag were able to inhibit the SOD activity but only the former had led to a significant increase in the mitochondrial superoxide. This suggested that i-Ag treatment did not generate superoxide and the reduced SOD activity was still capable of maintaining the cellular redox balance. On the contrary, n-Ag treatment caused substantial superoxide production in the mitochondrion that could not be taken care by the impaired SOD activity. It is widely accepted that metal-based NMs, but not their ionic forms, can enter the cell actively by endocytosis and mainly end up in the lysosomes, causing destabilization of the organelle and sequential ROS production in the cell (Sabella et al. 2014). Yang et al. (2012)

showed that Ag NM exposure triggered cathepsins leakage from lysosomes in primary human monocytes, inducing mitochondrial superoxide which led to inflammasome formation (Yang et al. 2012). Similar mechanism of action was also suggested in our previous study (Poon et al. 2017). The elevated gene expression of SOD2 upon n-Ag exposure again marked the attempt of the cells to restore the impaired antioxidant defense.

Under oxidative stress, PUFAs containing at least two skipped dienes are prone to non-enzymatic oxidation by free radicals that generate the novel oxidative stress biomarker, F_2-IsoPs which has been associated to neurodegenerative and cardiovascular diseases in human (Durand et al. 2011). The unchanged levels of F_2-IsoPs suggest that no free radical oxidation of PUFA was triggered by any of the three nanoparticles and the overall oxidative stress was low in the exposed cells. Although n-Ag exposure triggered production of mitochondrial superoxide, it could not directly oxidize cellular lipids but had to be further converted to more reactive hydroxyl radical ($OH^{\bullet}$) to do so (Durand et al. 2011, Magder 2006). It was likely that the cell's attempt to boost the antioxidant systems with an increased cellular GSH pool had prevented the production of F_2-IsoPs. Overall, the results suggested that cells exposed to n-Ag were at the first stage of oxidative stress where they were trying to restore the antioxidant defense against the increasing ROS production.

One of the major concerns regarding NM toxicity is the potentially enhanced cellular entry because of their small size, which can cause harm in the cell (Beddoes et al. 2015). Ion release is another important factor when considering the cellular entry of metal-based nanoparticles, as ions cannot cross the cell membrane easily, but nanoparticles can enter passively or actively via endocytosis (Beddoes et al. 2015). Overall, we showed that the cellular particle dose is largely dependent on exposure duration and particle dissolution outside of the cell. Size had a rather slight effect but still higher cellular doses were observed with n-Ag and b-ZnO exposures compared to their counterparts at 24 h. This seems to be associated with higher inflammatory potential, although effects remained mainly at the transcriptional level in b-ZnO exposed cells. It is noteworthy that the cellular dose was actually higher in n-ZnO-exposed cells at 6 h than at 24 h, supporting the general believe of smaller size favoring cellular entry. However, cellular dose dropped drastically from 6 h to 24 h, where a Zn importer gene, ZIP10 was found to be down-regulated and the two Zn exporter genes, ZnT1 and ZnT2 were up-regulated. These genes are important in maintaining the Zn homeostasis (Kambe et al. 2015) and are responsive to increase in intracellular Zn ion concentrations (Asani et al. 2017). Previously, n-ZnO was suggested to mediate fast ion release mainly at 6 h, whereas a more sustained ion release happened by b-ZnO at both 6 h and 24 h (Poon et al. 2017). The fast ion release of n-ZnO leading to high intracellular Zn ion accumulation, might have triggered a net export of Zn ions out of the cell in order to maintain Zn homeostasis. The smaller decrease in cellular Zn concentration with b-ZnO exposure goes along with the idea of sustained and slower release of ions from b-ZnO. Similar disruption of ZIP (Zn importer) and ZnT (Zn exporter) gene expressions was also seen with n-Ag exposed cells, but here the cellular Ag dose increased over time instead. It is likely that these Zn transporters are involved in maintenance of the intracellular cationic homeostasis, and have a role in defending the intracellularly released Ag ions by n-Ag. However, the cellular dose

was much higher in cells treated with n-Ag compared to ZnO particles, likely to be due to the enhanced internalization of intact nanoparticles over dissolved ions. Such high cellular Ag dose would probably have exceeded the cellular buffering capacity for intracellular ions, and continued to increase regardless of the over-expression of ZnTs.

During infection and inflammation, cellular polyunsaturated fatty acids (PUFAs) may undergo oxidation to produce the important lipid signaling molecules, eicosanoids, either enzymatically by lipoxygenase (LOX), cyclooxygenase (COX) and cytochrome P450 (CYP) enzymes, or non-enzymatically by cellular ROS induced free radical chain reactions (Dennis and Norris 2015). In general, the tested nanoparticles did not cause severe enzymatic PUFA oxidation, probably because we used sub-toxic doses of the nanoparticles. Yet, we showed that n-Ag induced elevation in the 5-HETE : AA ratio at 24 h, implicating increasing 5-HETE production from AA oxygenation in the cell even at such low n-Ag concentration. 5-HETE is generated exclusively through the LOX pathway, especially by the 5-lipoxygenase (5-LOX) isoform. Inflammatory stimuli can activate purinergic receptor or toll-like receptor (TLR) to mobilize 5-LOX and/or cytosolic phospholipase A_2 ($cPLA_2$) to move from the cytosol to the nuclear membrane. At the nuclear membrane, AA is released by $cPLA_2$ and passed to 5-LOX by FLAP (Dennis and Norris 2015), which can be eventually converted to 5-HETE or leukotrienes, which both are pro-inflammatory chemoattractants but their actions are mediated through different receptors and signaling cascades (O'Flaherty et al. 1998, Powell and Rokach 2005). 5-HETE may be converted to the potent chemoattractant 5-oxo-ETE under respiratory burst, oxidative stress and cell death. Both oxidized lipids are recognized by the G-protein coupled receptor OXE to mediate inflammatory and chemotactic responses. In particular, eosinophils have been suggested as the primary target of 5-oxo-ETE (Powell and Rokach 2013). Here, we did not see signs of specific eosinophils chemotaxis based on the microarray data. Considering the rather gentle status of oxidative stress, it was likely that 5-HETE was still the predominate form inside of cells exposed to n-Ag at 24 h. Some 5-HETEs are found esterified in the nuclear and non-nuclear membranes, which are functionally distinct from the free 5-HETEs. Clark et al. showed that stimulation by N-formyl-methionine-leucine-phenylalanine and priming with cytochalasin B, GM-CSF, or LPS triggers fast formation of esterified 5-HETE which could enhance superoxide and IL-8 production in neutrophils (Clark et al. 2011). In the current study, we have also found increasing levels of mitochondrial superoxide and a set of differentially expressed chemokine genes (CCL3, CXCL2, CXCL1, CXCL3 and CCL17) exclusively induced by exposure to n-Ag. Previously, we showed that n-Ag caused vast, statistically significant transcriptomic changes in differentiated THP-1 cells when compared to non-stimulated controls. In particular, the specific differentially expressed genes were mainly involved in type I interferon antiviral response likely via TLR7 activation, inflammasome activation and chemotaxis (Poon et al. 2017). Notwithstanding here, we showed exclusive induction of cellular 5-HETE production by exposure to n-Ag. It is likely that these responses are linked and collaborating to orchestra more severe inflammation in the cell compared to the other nanoparticles.

Interestingly, although cellular 5-HETE production was increased by n-Ag exposure, genes involved in the 5-LOX pathway, including, 5-LOX itself and FLAP, which activates 5-LOX, were down-regulated, maybe as a feed-back response to the increased 5-HETE level. On the contrary, the gene expression of COX-2 was significantly increased in cells treated with n-Ag. This could be explained by the differences in activation mechanisms of these enzymes. Upon cell stimulation, pre-existing $cPLA_2$ and 5-LOX are activated through calcium-dependent translocation and phosphorylation, which do not require gene induction and occur rapidly. The activity of the low expressing COX-2 however requires transcriptional activation and *de novo* protein synthesis, which are more time-consuming (Gimenez-Bastida et al. 2017). Because of the time lag in actions of the two pathways, and although no COX-2 oxidized products were found to be increased in the treated cell, we cannot exclude their potential generation at later time points.

So far, very few studies have looked into the potential link between NMs and PUFA oxidation/eicosanoids production in cells and none of the studies have related toxicity of Ag NMs to 5-HETE induction to the best of our knowledge. We have tested toxicity of all the used particles and their dose response at three different concentrations at the two timepoints (6 h and 24 h) in our previous article (Poon et al. 2017). However, to limit and focus this study, we have now used only the concentration causing low cytotoxicity (<15%) both in array and in lipidomic studies *in vitro*. This is also a study limitation, since the real human exposures might occur to lower concentrations and last much longer. However, this study sheds more light on both the mechanism of action of Ag NMs and the roles of 5-HETE during inflammation, which are less well defined compared to leukotrienes, which are also generated by the 5-LOX pathway (Dennis and Norris 2015). Putting all the data together, we proposed that n-Ag are internalized by macrophages, leading to low level of oxidative stress through both ROS production and antioxidant disruption in the cell, triggering the restoration of antioxidant defense. On the other hand, n-Ag induces inflammation, stimulating AA oxidation to form 5-HETE, which further magnifies the inflammatory responses by enhancing the production of mitochondrial superoxide and leukocyte chemokines (Fig. 6). Such effects are expected to be long-lasting considering the sustained n-Ag uptake detected.

List of abbreviations

NM, nanomaterial; PBS, phosphate buffered saline; ROS, reactive oxygen-species; PUFA, polyunsaturated fatty acids; LC/MS, Liquid chromatography–mass spectrometry; GSH, glutathione; GSSG, oxidized form of glutathione; SOD, superoxide dismutase; AA, arachidonic acids; EPA, eicosapentaenoic acid; DHA, docosahexaenoic acid; LOX, lipoxygenases; COX, cyclooxygenases, CYP, cytochrome; HETE, hydroxyeicosatetraenoic acid; HDoHE, hydroxydocosahexaenoic acids; IsoP, isoprostane; cRPMI, complete RPMI medium; BHT, butylated hydroxytoluene; ICP-MS, Inductively coupled plasma mass spectrometry.

AA, Arachidonic acid; COX-2, Cyclooxygenase-2; FLAP also called ALOX5AP, Arachidonate 5-lipoxygenase-activating protein; GCLC, Glutamate-cysteine ligase, also known as gamma-

glutamylcysteine synthetase; GPX, Glutathione peroxidase; 5-HETE.5- Hydroxyeicosatetraenoic acid; 5-LOX, Arachidonate 5-Lipoxygenase; PLA2, Phospholipase A2; SOD, Superoxide dismutase; SOD2, Superoxide dismutase 2.

Availability of data and materials

The datasets supporting the conclusion of this article are included within the article and its additional files. By request, the microarray data produced in this study is available from piia.karisola@helsinki.fi, and the metabolomic data produced in this study is available from XXX.

Notes

The authors declare no competing financial interest. The authors alone are responsible for the content and writing of this article.

Acknowledgements

The study was supported by a grant from the Academy of Finland (decision 297885).

References

Asani, S. C., R. D. Umrani and K. M. Paknikar. 2017. “Differential dose-dependent effects of zinc oxide nanoparticles on oxidative stress-mediated pancreatic beta-cell death.” Nanomedicine (Lond) 12(7): 745-759. doi:10.2217/nnm-2016-0426.

Ballatori, N., S. M. Krance, R. Marchan and C. L. Hammond. 2009. “Plasma membrane glutathione transporters and their roles in cell physiology and pathophysiology.” Mol Aspects Med 30(1-2): 13-28. doi:10.1016/j.mam.2008.08.004.

Beddoes, C. M., C. P. Case and W. H. Briscoe. 2015. “Understanding nanoparticle cellular entry: A physicochemical perspective.” Adv Colloid Interface Sci 21848-68. doi:10.1016/j.cis.2015.01.007.

Cameron, S. J., F. Hosseinian and W. G. Willmore. 2018. “A Current Overview of the Biological and Cellular Effects of Nanosilver.” Int J Mol Sci 19(7). doi:10.3390/ijms19072030.

Chen, Q., N. Wang, M. Zhu, J. Lu, H. Zhong, X. Xue, S. Guo, M. Li, X. Wei, Y. Tao and H. Yin. 2018. “TiO2 nanoparticles cause mitochondrial dysfunction, activate inflammatory responses, and attenuate phagocytosis in macrophages: A proteomic and metabolomic insight.” Redox Biol 15266-276. doi:10.1016/j.redox.2017.12.011.

Ciriolo, M. R., P. Civitareale, M. T. Carri, A. De Martino, F. Galiazzo and G. Rotilio. 1994. “Purification and characterization of Ag,Zn-superoxide dismutase from Saccharomyces cerevisiae exposed to silver.” J Biol Chem 269(41): 25783-25787.

Clark, S. R., C. J. Guy, M. J. Scurr, P. R. Taylor, A. P. Kift-Morgan, V. J. Hammond, C. P. Thomas, B. Coles, G. W. Roberts, M. Eberl, S. A. Jones, N. Topley, S. Kotecha and V. B. O'Donnell. 2011. “Esterified eicosanoids are acutely generated by 5-lipoxygenase in primary human neutrophils and in human and murine infection.” Blood 117(6): 2033-2043. doi:10.1182/blood-2010-04-278887.

Dennis, E. A. and P. C. Norris. 2015. “Eicosanoid storm in infection and inflammation.” Nat Rev Immunol 15(8): 511-523. doi:10.1038/nri3859.

DTU Environment, t. D. E. C. a. D. C. C. The Nanodatabase. Journal [Online] Available at: http://nanodb.dk.

Dupuy, A., P. Le Faouder, C. Vigor, C. Oger, J. M. Galano, C. Dray, J. C. Lee, P. Valet, C. Gladine, T. Durand and J. Bertrand-Michel. 2016. “Simultaneous quantitative profiling of 20 isoprostanoids from omega-3 and omega-6 polyunsaturated fatty acids by LC-MS/MS in various biological samples.” Anal Chim Acta 92146-58. doi:10.1016/j.aca.2016.03.024.

Durand, T., V. Bultel-Ponce, A. Guy, S. El Fangour, J. C. Rossi and J. M. Galano. 2011. “Isoprostanes and phytoprostanes: Bioactive lipids.” Biochimie 93(1): 52-60. doi:10.1016/j.biochi.2010.05.014.

Fu, P. P., Q. Xia, H. M. Hwang, P. C. Ray and H. Yu. 2014. “Mechanisms of nanotoxicity: generation of reactive oxygen species.” J Food Drug Anal 22(1): 64-75. doi:10.1016/j.jfda.2014.01.005.

Fukai, T. and M. Ushio-Fukai. 2011. “Superoxide dismutases: role in redox signaling, vascular function, and diseases.” Antioxid Redox Signal 15(6): 1583-1606. doi:10.1089/ars.2011.3999.

Funk, C. D. 2001. “Prostaglandins and leukotrienes: advances in eicosanoid biology.” Science 294(5548): 1871-1875. doi:10.1126/science.294.5548.1871.

Gimenez-Bastida, J. A., T. Shibata, K. Uchida and C. Schneider. 2017. “Roles of 5-lipoxygenase and cyclooxygenase-2 in the biosynthesis of hemiketals E2 and D2 by activated human leukocytes.” FASEB J 31(5): 1867-1878. doi:10.1096/fj.201601136R.

Hernandez, L. E., J. Sobrino-Plata, M. B. Montero-Palmero, S. Carrasco-Gil, M. L. Flores-Caceres, C. Ortega-Villasante and C. Escobar. 2015. “Contribution of glutathione to the control of cellular redox homeostasis under toxic metal and metalloid stress.” J Exp Bot 66(10): 2901-2911. doi:10.1093/jxb/erv063.

Huang, Y., M. Zhu, Z. Li, R. Sa, Q. Chu, Q. Zhang, H. Zhang, W. Tang, M. Zhang and H. Yin. 2014. “Mass spectrometry-based metabolomic profiling identifies alterations in salivary redox status and fatty acid metabolism in response to inflammation and oxidative stress in periodontal disease.” Free Radic Biol Med 70223-232. doi:10.1016/j.freeradbiomed.2014.02.024.

Kambe, T., T. Tsuji, A. Hashimoto and N. Itsumura. 2015. “The Physiological, Biochemical, and Molecular Roles of Zinc Transporters in Zinc Homeostasis and Metabolism.” Physiol Rev 95(3): 749-784. doi:10.1152/physrev.00035.2014.

Khanna, P., C. Ong, B. H. Bay and G. H. Baeg. 2015. “Nanotoxicity: An Interplay of Oxidative Stress, Inflammation and Cell Death.” Nanomaterials (Basel) 5(3): 1163-1180. doi:10.3390/nano5031163.

Kreyling, W. G., M. Semmler-Behnke, J. Seitz, W. Scymczak, A. Wenk, P. Mayer, S. Takenaka and G. Oberdorster. 2009. “Size dependence of the translocation of inhaled iridium and carbon nanoparticle aggregates from the lung of rats to the blood and secondary target organs.” Inhal Toxicol 21 Suppl 155-60. doi:10.1080/08958370902942517.

Leung, B. O., F. Jalilehvand, V. Mah, M. Parvez and Q. Wu. 2013. “Silver(I) complex formation with cysteine, penicillamine, and glutathione.” Inorg Chem 52(8): 4593-4602. doi:10.1021/ic400192c.

Magder, S. 2006. “Reactive oxygen species: toxic molecules or spark of life?” Crit Care 10(1): 208. doi:10.1186/cc3992.

Nel, A., T. Xia, L. Madler and N. Li. 2006. “Toxic potential of materials at the nanolevel.” Science 311(5761): 622-627. doi:10.1126/science.1114397.

O'Flaherty, J. T., J. S. Taylor and M. J. Thomas. 1998. “Receptors for the 5-oxo class of eicosanoids in neutrophils.” J Biol Chem 273(49): 32535-32541.

Palomaki, J., E. Valimaki, J. Sund, M. Vippola, P. A. Clausen, K. A. Jensen, K. Savolainen, S. Matikainen and H. Alenius. 2011. “Long, needle-like carbon nanotubes and asbestos activate the NLRP3 inflammasome through a similar mechanism.” ACS Nano 5(9): 6861-6870. doi:10.1021/nn200595c.

Pietroiusti, A., L. Campagnolo and B. Fadeel. 2013. “Interactions of engineered nanoparticles with organs protected by internal biological barriers.” Small 9(9-10): 1557-1572. doi:10.1002/smll.201201463.

Pietroiusti, A., H. Stockmann-Juvala, F. Lucaroni and K. Savolainen. 2018. “Nanomaterial exposure, toxicity, and impact on human health.” Wiley Interdiscip Rev Nanomed Nanobiotechnol. doi:10.1002/wnan.1513.

Poon, W. L., H. Alenius, J. Ndika, V. Fortino, V. Kolhinen, A. Mesceriakovas, M. Wang, D. Greco, A. Lahde, J. Jokiniemi, J. C. Lee, H. El-Nezami and P. Karisola. 2017. "Nano-sized zinc oxide and silver, but not titanium dioxide, induce innate and adaptive immunity and antiviral response in differentiated THP-1 cells." Nanotoxicology 11(7): 936-951. doi:10.1080/17435390.2017.1382600.

Powell, W. S. and J. Rokach. 2005. "Biochemistry, biology and chemistry of the 5-lipoxygenase product 5-oxo-ETE." Prog Lipid Res 44(2-3): 154-183. doi:10.1016/j.plipres.2005.04.002.

Powell, W. S. and J. Rokach. 2013. "The eosinophil chemoattractant 5-oxo-ETE and the OXE receptor." Prog Lipid Res 52(4): 651-665. doi:10.1016/j.plipres.2013.09.001.

Qin, Z. Y. 2012. "The use of THP-1 cells as a model for mimicking the function and regulation of monocytes and macrophages in the vasculature." Atherosclerosis 221(1): 2-11. doi:10.1016/j.atherosclerosis.2011.09.003.

Sabella, S., R. P. Carney, V. Brunetti, M. A. Malvindi, N. Al-Juffali, G. Vecchio, S. M. Janes, O.M. Bakr, R. Cingolani, F. Stellacci and P. P. Pompa. 2014. "A general mechanism for intracellular toxicity of metal-containing nanoparticles." Nanoscale 6(12):7052-61. doi: 10.1039/c4nr01234h.

Sharifi, S., S. Behzadi, S. Laurent, M. L. Forrest, P. Stroeve and M. Mahmoudi. 2012. "Toxicity of nanomaterials." Chem Soc Rev 41(6): 2323-2343. doi:10.1039/c1cs15188f.

Sies, H. (1985). 1 - Oxidative Stress: Introductory Remarks. In: H. Sies ed. Oxidative Stress. London: Academic Press, 1-8.

Vance, M. E., T. Kuiken, E. P. Vejerano, S. P. McGinnis, M. F. Hochella, Jr., D. Rejeski and M. S. Hull. 2015. "Nanotechnology in the real world: Redeveloping the nanomaterial consumer products inventory." Beilstein J Nanotechnol 61769-1780. doi:10.3762/bjnano.6.181.

Wu, G., Y. Z. Fang, S. Yang, J. R. Lupton and N. D. Turner. 2004. "Glutathione metabolism and its implications for health." J Nutr 134(3): 489-492. doi:10.1093/jn/134.3.489.

Xu, P., L. Liu, G. Zeng, D. Huang, C. Lai, M. Zhao, C. Huang, N. Li, Z. Wei, H. Wu, C. Zhang, M. Lai and Y. He. 2014. "Heavy metal-induced glutathione accumulation and its role in heavy metal detoxification in Phanerochaete chrysosporium." Appl Microbiol Biotechnol 98(14): 6409-6418. doi:10.1007/s00253-014-5667-x.

Yang, E. J., S. Kim, J. S. Kim and I. H. Choi. 2012. "Inflammasome formation and IL-1beta release by human blood monocytes in response to silver nanoparticles." Biomaterials 33(28): 6858-6867. doi:10.1016/j.biomaterials.2012.06.016.

Yin, H., Y. Zhou, M. Zhu, S. Hou, Z. Li, H. Zhong, J. Lu, T. Meng, J. Wang, L. Xia, Y. Xu and Y. Wu. 2013. "Role of mitochondria in programmed cell death mediated by arachidonic acid-derived eicosanoids." Mitochondrion 13(3): 209-224. doi:10.1016/j.mito.2012.10.003.

Figure legends

Figure 1. Changes in cellular antioxidants and mitochondrial superoxides were measured 6 h and 24 h after the exposure to nano-sized ZnO (n-ZnO), n-TiO_2 and n-Ag and their bulk-sized (b-TiO_2, b-ZnO) or ionic (i-Ag) counterparts. (A) Total cellular glutathione (GSH) was measured by glutathione assay (n=5 replicas). (B) Based on gene expression arrays (n=3 replicas), glutamate-cysteine ligase (GCLC) expression accompanied the observed changes of total GSH. (C) Superoxide dismutase activity (SOD) showed reduced activity for n-Ag and i-Ag in SOD assay at 24 h (n=5 replicas). (D) Produced superoxide in mitochondria (Mt superoxide) was selectively stained with MitoSox Red and studied by confocal laser scanning microscopy (n=4 replicas). (E) Also, expression of mitochondrial superoxide dismutase 2 (SOD2) was highly upregulated by b-ZnO and n-Ag in gene expression arrays at both time points. Results are expressed as mean ± SD in A, D and D. Significance indicated by *p < 0.05, **p < 0.01, ***p < 0.001, ****p < 0.0001 determined by one-way ANOVA.

Figure 2. Cellular particle dose, and gene expression of zinc transporters at 6 h or 24 h after the exposures. Particle uptake was measured by ICP-MS as a concentration of (A) Ti, (B) Zn and (C) Ag in the cell samples exposed to n/b-TiO_2, n/b-ZnO and n/i-Ag for 6 or 24 h. The concentrations are expressed as mean ± SD of three replicates with the background level (in unexposed control group) subtracted. (D) Downregulation of a zinc importer gene ZIP10, and concomitant (E) upregulation of two zinc ion exporter genes (ZnT1 and ZnT2) were induced by n/b-ZnO and n-Ag at both 6 h and 24 h, measured by gene expression microarrays. Significance indicated by *p < 0.05, **p < 0.01, ***p < 0.001, ****p < 0.0001 and determined by two-way ANOVA.

Figure 3. Effects of TiO_2, ZnO and Ag nanoparticles and corresponding control particles on PUFA metabolism in THP-1 cells after 24 h of exposure. (A) Schematic representation of enzymatic oxidation of PUFAs, with major oxidized metabolites bolded, measured metabolites highlighted in yellow, detectable metabolites in red text and enzymes participated italicized and color coded (COXs in green, LOXs in purple, CYPs in orange-brown). (B) N-Ag significantly increased the ratio of 5-HETE to its precursor PUFA, AA, at 24 h, indicating 5-LOX-mediated oxidation of AA to form the pro-inflammatory 5-HETE. (C) The ratio of free radical generated F2-IsoPs to precursor AA remained unchanged regardless of the type of nanoparticles received by the cell. Results are expressed as mean ± SD (n = 5). Significance indicated by *p < 0.05, **p < 0.01, ***p < 0.001, ****p < 0.0001 determined by one-way ANOVA.

Figure 4. Changes in gene expression of phospholipase A2 (PLA2) and enzymes involved in the oxidation of polyunsaturated fatty acids (PUFAs) including lipoxygenase (LOX, FLAP) and cyclooxygenase (COX) 6 h or 24 h after the particle exposures in THP-1 cells. (A) Phospholipase A2 isozyme PLA2G4C, (B) 5-LOX and (C) 5-LOX activating genes FLAP (called also ALOX5AP), and (D) COX-2 genes (called also PTGS2) are differentially expressed after exposure to different

particles in the gene expression arrays. Individual values are shown (n = 3). Significance indicated by *p < 0.05, **p < 0.01, ***p < 0.001, ****p < 0.0001 determined by one-way ANOVA.

Figure 5. Gene expression of chemotaxis-related genes (CCL3, CXCL1-3, CCL17) in THP-1 cells 6 h and 24 h after the NM exposures. (A) B/n-ZnO and n-Ag enhance chemotaxis of polymorphonuclear leukocytes, especially neutrophils, by increasing the expression of CCL3, CXCL2 and CXCL1 genes. (B) Also, chemotaxis for monocytes and T cells is induced by expression of CXCL3 and CCL17, respectively. Individual values shown (n=3) and significance indicated by *p < 0.05, **p < 0.01, ***p < 0.001, ****p < 0.0001 determined by one-way ANOVA.

Figure 6. Model of functions and effects of n-Ag on THP-1 cells. Integrating all the data of this study, it is proposed that n-Ag induces production of mitochondrial superoxide ($O_2^{\bullet -2}$, H_2O_2) 5-HETE and chemokines, which lead to sustained inflammation and chemotaxis.
AA, Arachidonic acid; COX-2, Cyclooxygenase-2; FLAP also called ALOX5AP, Arachidonate 5-lipoxygenase-activating protein; GCLC, Glutamate-cysteine ligase, also known as gamma-glutamylcysteine synthetase; GPX, Glutathione peroxidase; 5-HETE.5- Hydroxyeicosatetraenoic acid; 5-LOX, Arachidonate 5-Lipoxygenase; PLA2, Phospholipase A2; SOD, Superoxide dismutase; SOD2, Superoxide dismutase 2.

Tables

Table 1. Relationship between cellular uptake and particle dissolution in medium. The insoluble n/b-TiO_2 and hardly soluble n-Ag exhibited much higher cellular uptake compared to the readily dissolving n/b-ZnO and soluble $AgNO_3$ (i-Ag). % cellular uptake of nanoparticles was calculated by absolute cellular dose (determined by ICP-MS, Fig. 2) over the administrated particle dose (i.e. 59934 ppb Ti, 8034 ppb Zn and 10000 ppb Ag). The percent of dissolution (% dissolution) is referred to percentage of the administrated particle dissolved in the acellular medium determined by ICP-MS. The nano- and bulk-sized particles were incubated in medium without cells for 24 h and the released ions were captured in the supernatant after centrifugation.

	% cellular uptake		**% dissolution**
	6 h	**24 h**	**6 h**
n-TiO_2	34.1	50.7	< detection limit
b-TiO_2	32.7	44.9	< detection limit
n-ZnO	8.6	4.1	51.9
b-ZnO	7.2	5.5	58.4
n-Ag	15.2	35.5	1.7
i-Ag	2.7	5.0	N/A

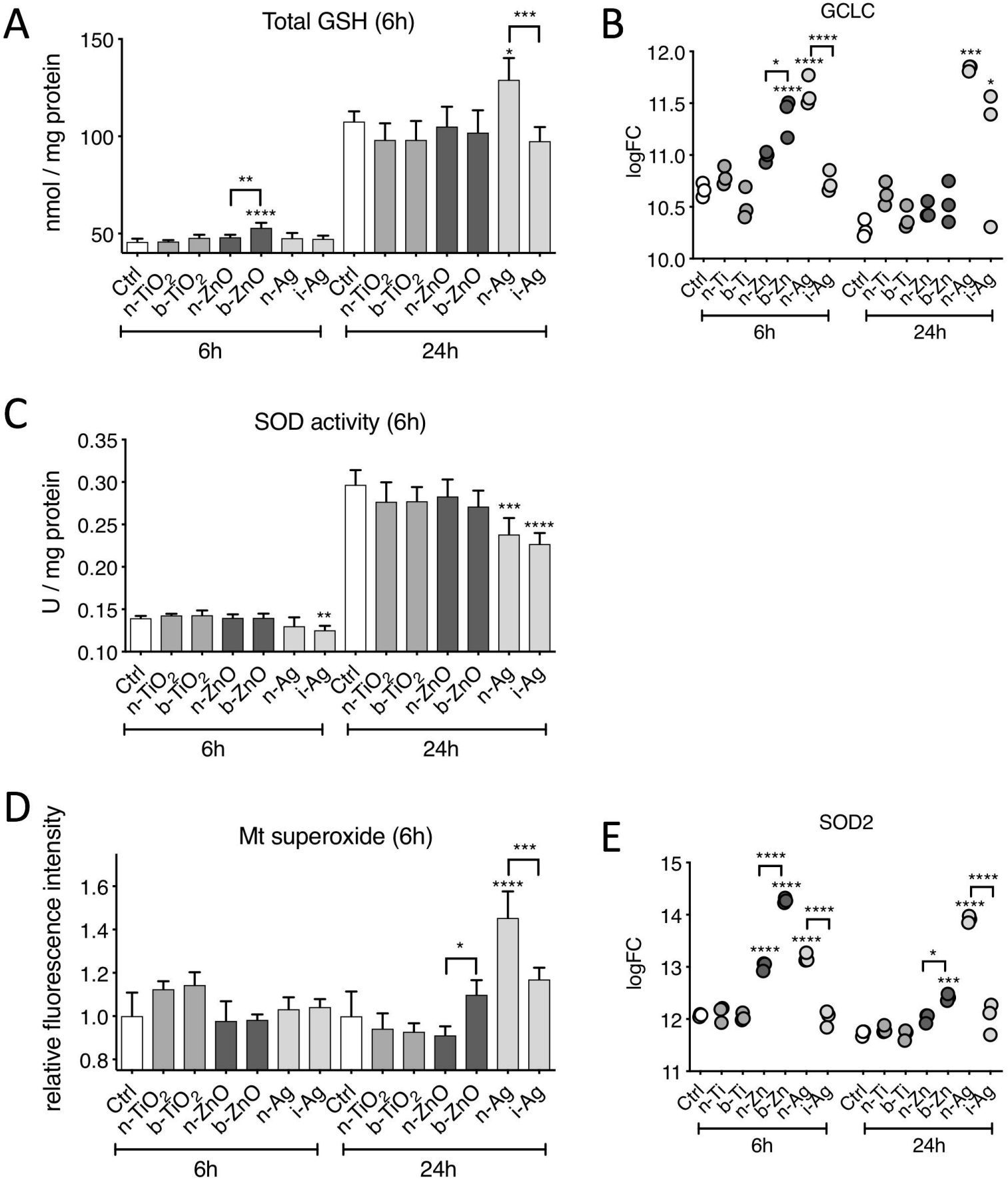
A
Total GSH (6h)
nmol / mg protein
150
100
50
Ctrl
n-TiO2
b-TiO2
n-ZnO
b-ZnO
n-Ag
i-Ag
6h
24h
B
GCLC
logFC
12.0
11.5
11.0
10.5
10.0
Ctrl
n-Ti
b-Ti
n-Zn
b-Zn
n-Ag
i-Ag
6h
24h
C
SOD activity (6h)
U / mg protein
0.35
0.30
0.25
0.20
0.15
0.10
D
Mt superoxide (6h)
relative fluorescence intensity
1.6
1.4
1.2
1.0
0.8
E
SOD2
logFC
15
14
13
12
11

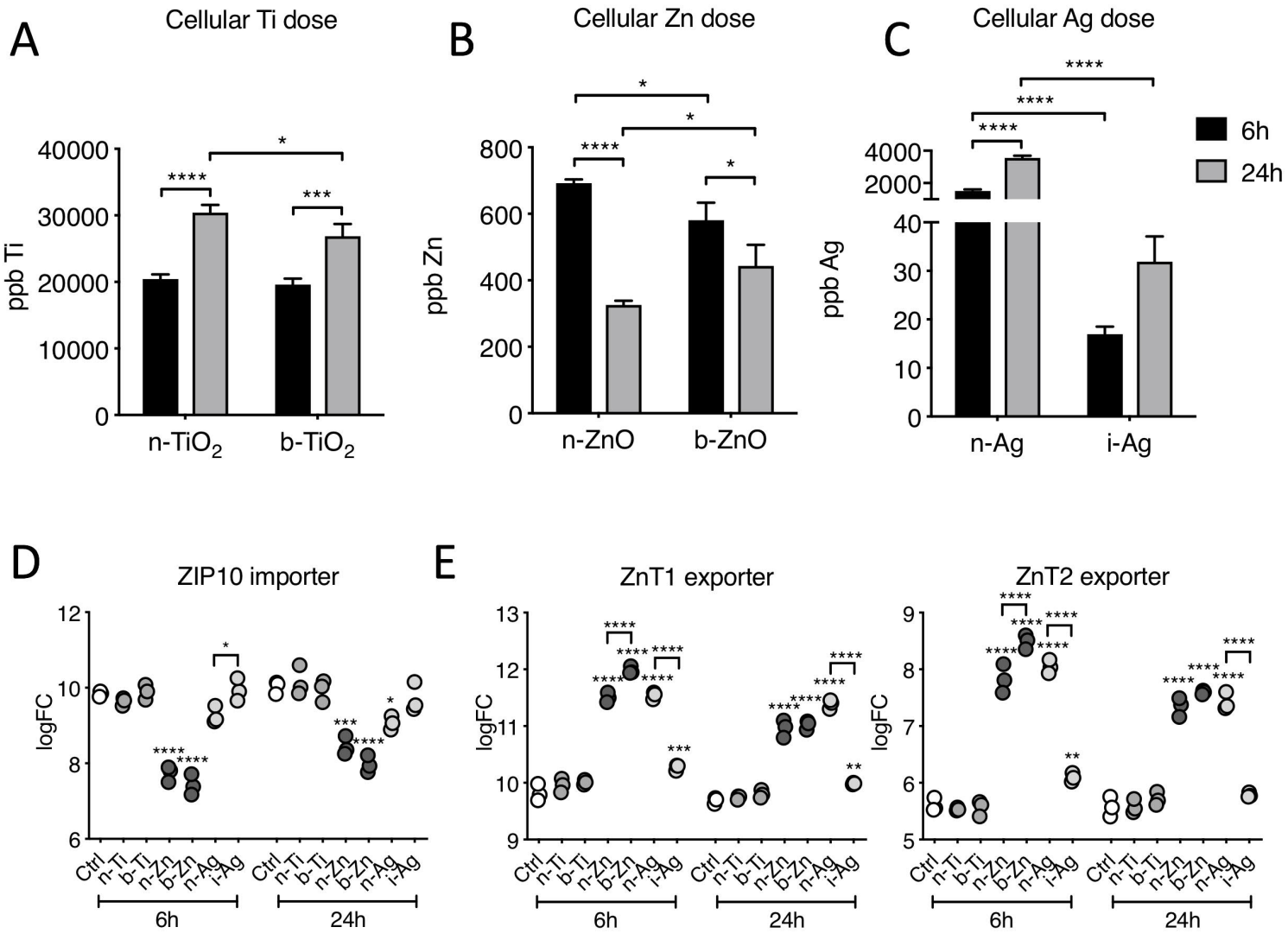
A
Cellular Ti dose
ppb Ti
40000
30000
20000
10000
0
n-TiO2
b-TiO2
B
Cellular Zn dose
ppb Zn
800
600
400
200
0
n-ZnO
b-ZnO
C
Cellular Ag dose
ppb Ag
4000
2000
40
30
20
10
0
n-Ag
i-Ag
6h
24h
D
ZIP10 importer
logFC
12
10
8
6
E
ZnT1 exporter
13
12
11
10
9
ZnT2 exporter
9
8
7
6
5
Ctrl
n-Ti
b-Ti
n-Zn
b-Zn
n-Ag
i-Ag
6h
24h

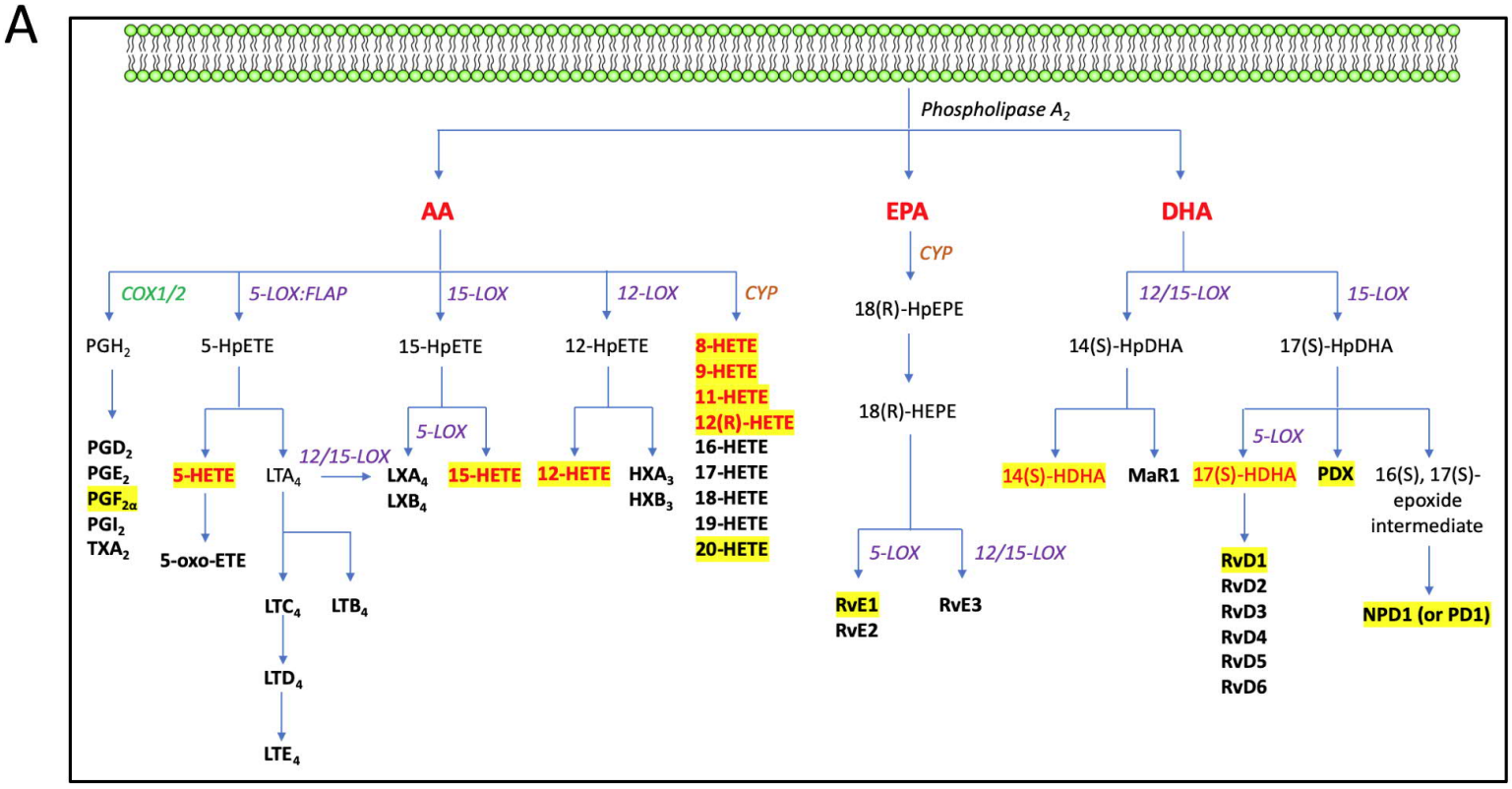
A
Phospholipase A2
AA
EPA
DHA
CYP
COX1/2
5-LOX:FLAP
15-LOX
12-LOX
CYP
12/15-LOX
15-LOX
PGH2
5-HpETE
15-HpETE
12-HpETE
8-HETE
9-HETE
11-HETE
12(R)-HETE
16-HETE
17-HETE
18-HETE
19-HETE
20-HETE
18(R)-HpEPE
18(R)-HEPE
14(S)-HpDHA
17(S)-HpDHA
PGD2
PGE2
PGF2α
PGI2
TXA2
5-HETE
LTA4
12/15-LOX
LXA4
LXB4
15-HETE
12-HETE
HXA3
HXB3
5-LOX
14(S)-HDHA
MaR1
17(S)-HDHA
PDX
16(S), 17(S)-epoxide intermediate
5-oxo-ETE
LTC4
LTB4
LTD4
LTE4
RvE1
RvE2
RvE3
RvD1
RvD2
RvD3
RvD4
RvD5
RvD6
NPD1 (or PD1)

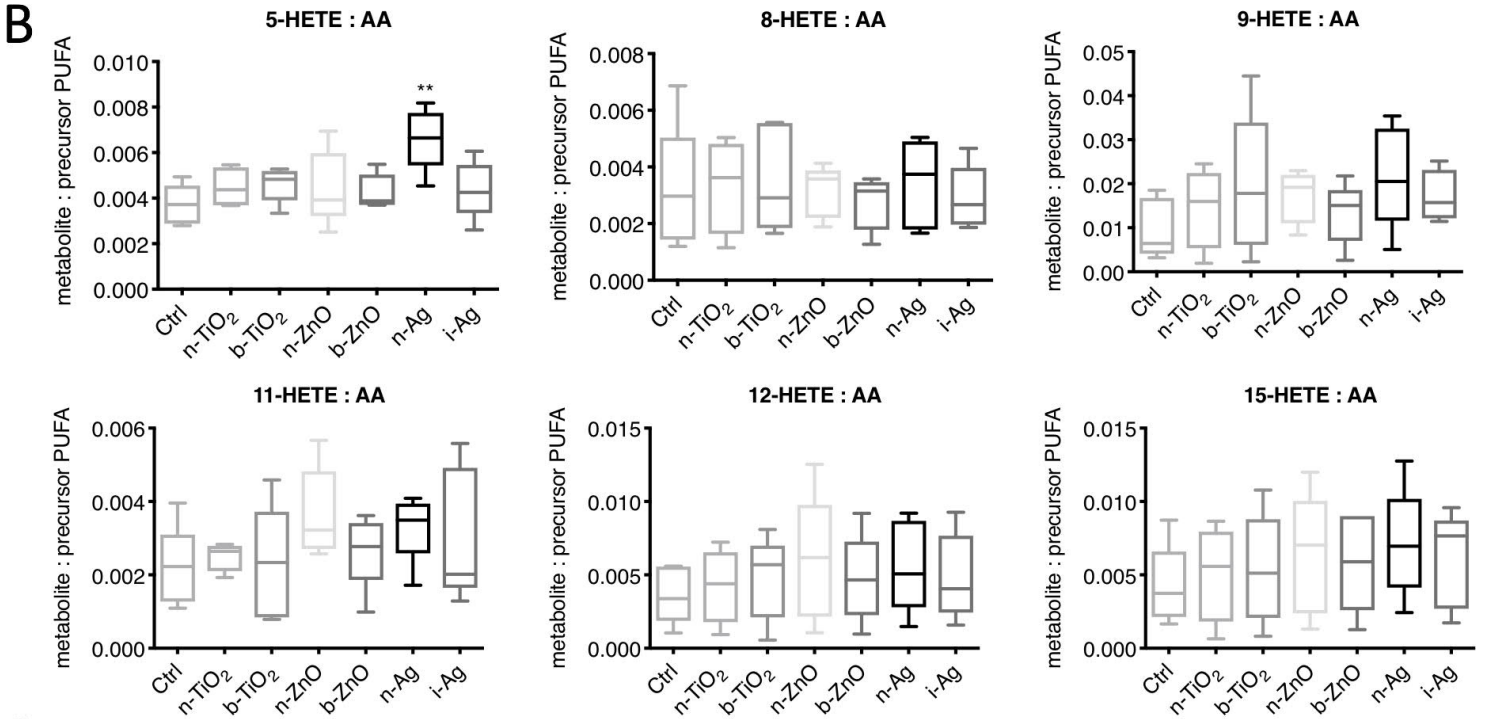
B
5-HETE : AA
8-HETE : AA
9-HETE : AA
11-HETE : AA
12-HETE : AA
15-HETE : AA
metabolite : precursor PUFA
**
Ctrl
n-TiO2
b-TiO2
n-ZnO
b-ZnO
n-Ag
i-Ag

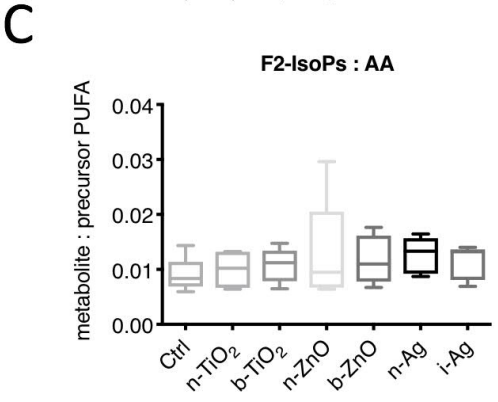
C
F2-IsoPs : AA
metabolite : precursor PUFA
Ctrl
n-TiO2
b-TiO2
n-ZnO
b-ZnO
n-Ag
i-Ag

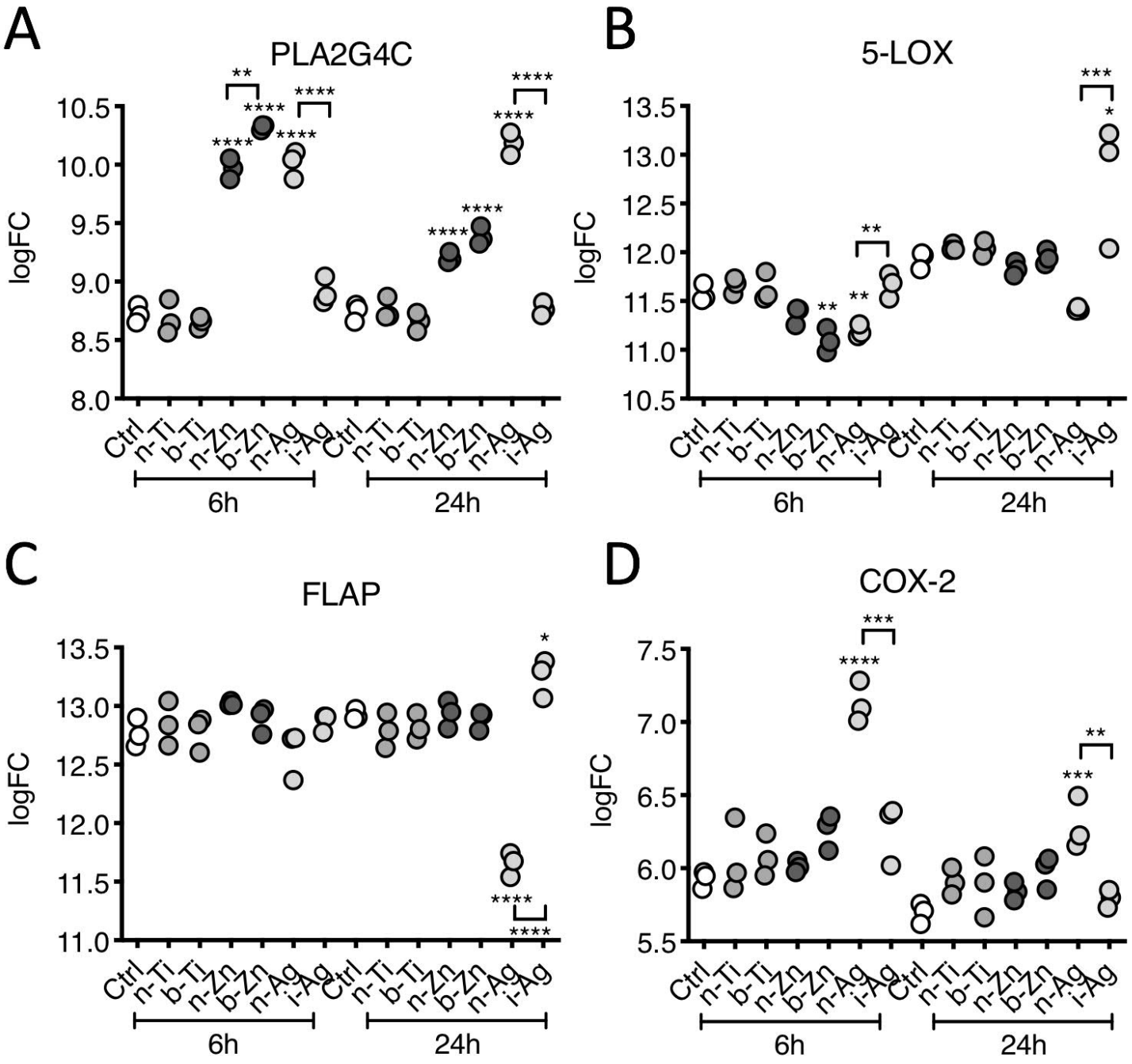
A
PLA2G4C
logFC
10.5
10.0
9.5
9.0
8.5
8.0
Ctrl
n-Ti
b-Ti
n-Zn
b-Zn
n-Ag
i-Ag
6h
24h
B
5-LOX
logFC
13.5
13.0
12.5
12.0
11.5
11.0
10.5
C
FLAP
logFC
13.5
13.0
12.5
12.0
11.5
11.0
D
COX-2
logFC
7.5
7.0
6.5
6.0
5.5

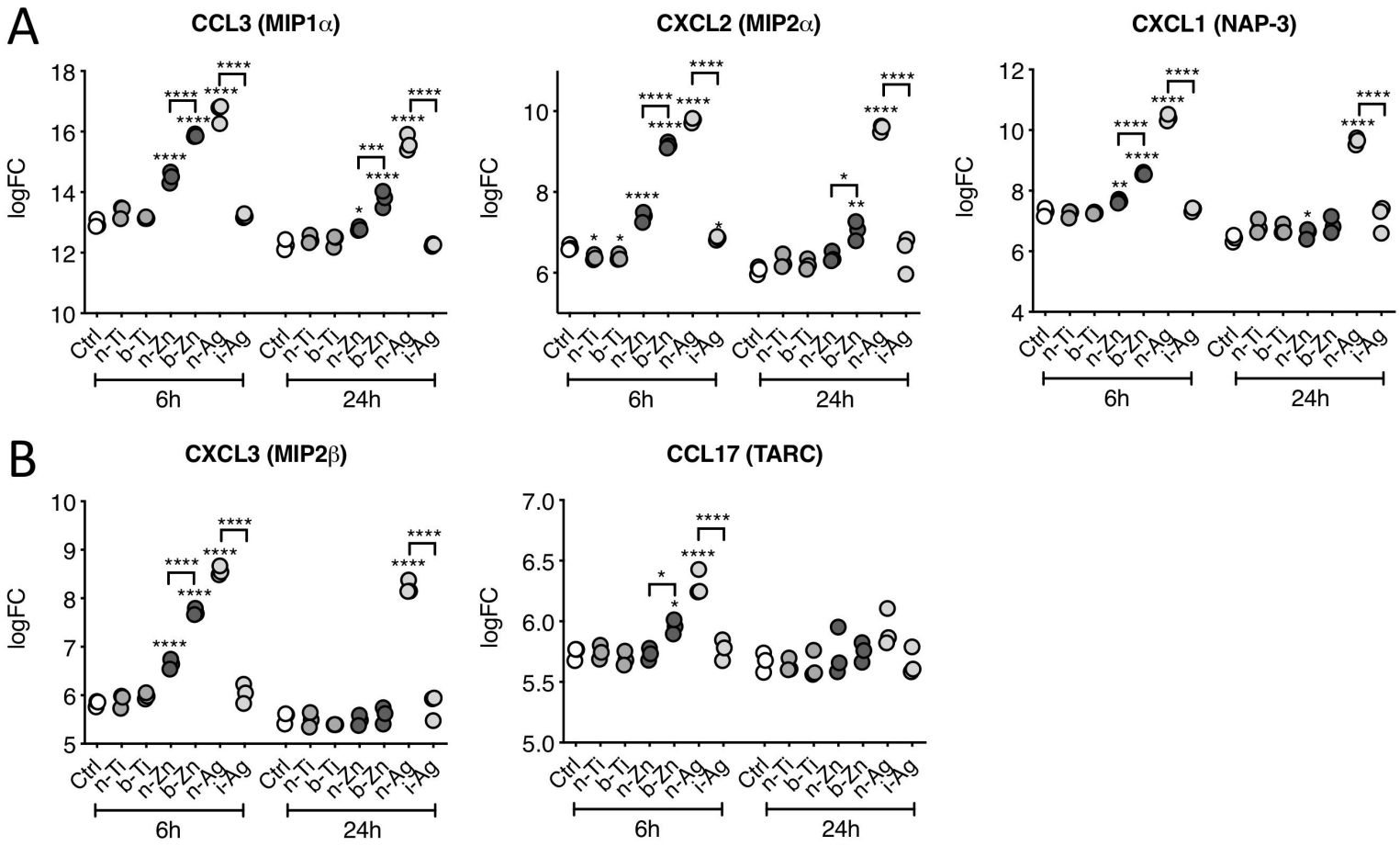
A
CCL3 (MIP1α)
CXCL2 (MIP2α)
CXCL1 (NAP-3)
B
CXCL3 (MIP2β)
CCL17 (TARC)
logFC
Ctrl
n-Ti
b-Ti
n-Zn
b-Zn
n-Ag
i-Ag
6h
24h

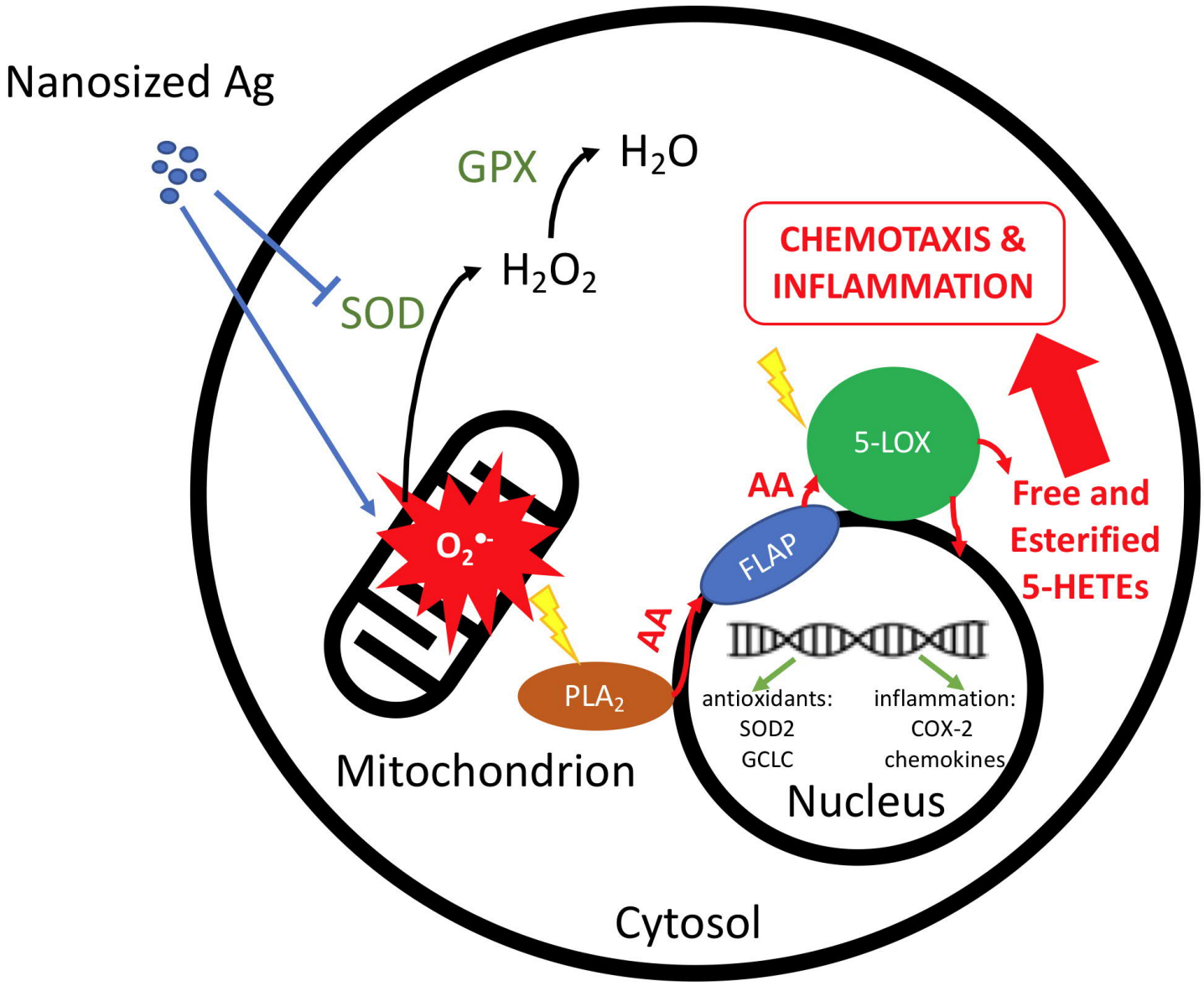
Nanosized Ag
GPX
H_2O
H_2O_2
SOD
CHEMOTAXIS &
INFLAMMATION
5-LOX
AA
Free and
Esterified
5-HETEs
FLAP
$O_2^{\bullet-}$
AA
PLA_2
antioxidants:
SOD2
GCLC
inflammation:
COX-2
chemokines
Mitochondrion
Nucleus
Cytosol

Supplementary Material for:

Nanosized silver, but not titanium dioxide or zinc oxide, enhances oxidative stress and inflammatory response by inducing 5-HETE activation in THP-1 cells

Wing-Lam Poon,[1]* Jetty Chung-Yung Lee,[1]* Kin Sum Leung[1], Harri Alenius,[2,3] Hani El-Nezami,[1,4§] Piia Karisola[2§]

[1]School of Biological Sciences, University of Hong Kong, Pokfulam Road, Hong Kong
[2]Human Microbiome Research Program, University of Helsinki, Haartmaninkatu 3, 00290 Helsinki, Finland
[3]Institute of Environmental Medicine (IMM), Karolinska Institutet, Stockholm 171 77, Sweden
[4]Nutrition and health, Institute of Public Health and Clinical Nutrition, University of Eastern Finland, P.O. Box 1627, 70211 Kuopio, Finland

*These authors contributed equally to this work.
[§]Address correspondence to piia.karisola@helsinki.fi and elnezami@hku.hk

6h	Ctrl	n-TiO_2	b-TiO_2	n-ZnO	b-ZnO	n-Ag	i-Ag
Polyunsaturated fatty acids (PUFAs)							
AA (ng/mg protein)	189.86 ± 34.52	208.71 ± 21.12	221.46 ± 64.80	177.36 ± 38.23	230.08 ± 27.47	165.94 ± 42.48	185.86 ± 55.11
AdA (ng/mg protein)	29.73 ± 11.00	30.79 ± 11.97	33.70 ± 7.85	30.77 ± 13.50	32.11 ± 10.17	24.80 ± 11.09	26.07 ± 14.89
DHA (ng/mg protein)	0.196 ± 0.062	0.251 ± 0.061	0.187 ± 0.025	0.186 ± 0.039	0.205 ± 0.042	0.137 ± 0.040	0.141 ± 0.058
DPA (ng/mg protein)	616.31 ± 240.48	827.23 ± 364.45	658.72 ± 133.66	660.76 ± 218.60	654.77 ± 112.22	494.41 ± 130.41	597.43 ± 399.39
EPA (ng/mg protein)	12160.13 ± 5208.53	14607.68 ± 7794.39	16070.10 ± 10408.98	14123.28 ± 7246.06	18642.42 ± 9716.05	11116.70 ± 4237.84	10043.44 ± 3859.69
Enzymatically oxidized lipid metabolites							
5-HETE : AA	0.00469 ± 0.00168	0.00567 ± 0.00195	0.00487 ± 0.00118	0.00397 ± 0.00129	0.00465 ± 0.00082	0.00495 ± 0.00193	0.00416 ± 0.00131
8-HETE : AA	0.00298 ± 0.00127	0.00300 ± 0.00055	0.00254 ± 0.00129	0.00258 ± 0.00083	0.00277 ± 0.00047	0.00278 ± 0.00129	0.00225 ± 0.00051
9-HETE : AA	0.01772 ± 0.00485	0.01698 ± 0.00545	0.01064 ± 0.00857	0.02065 ± 0.00954	0.01947 ± 0.00725	0.02257 ± 0.01478	0.01062 ± 0.00286
11-HETE : AA	0.00279 ± 0.00122	0.00296 ± 0.00117	0.00280 ± 0.00158	0.00247 ± 0.00178	0.00312 ± 0.00122	0.00259 ± 0.00180	0.00195 ± 0.00075
12-HETE : AA	0.00699 ± 0.00200	0.00601 ± 0.00191	0.00665 ± 0.00292	0.00805 ± 0.00258	0.00711 ± 0.00281	0.00843 ± 0.00486	0.00648 ± 0.00213
15-HETE : AA	0.00714 ± 0.00243	0.00885 ± 0.00417	0.00713 ± 0.00315	0.00823 ± 0.00229	0.00926 ± 0.00363	0.00944 ± 0.00389	0.00747 ± 0.00188
4-HDoHE : DHA	11.54 ± 4.21	14.44 ± 7.10	14.30 ± 4.28	9.04 ± 1.47	9.91 ± 1.88	13.20 ± 5.41	17.67 ± 8.55
7-HDoHE : DHA	2.41 ± 1.01	2.67 ± 1.16	3.51 ± 0.48	1.98 ± 0.77	2.45 ± 0.74	2.88 ± 0.90	4.27 ± 2.47
8-HDoHE : DHA	17.23 ± 6.47	20.76 ± 9.33	22.13 ± 13.10	18.85 ± 7.89	23.50 ± 8.68	25.43 ± 11.32	25.71 ± 4.94
11-HDoHE : DHA	8.72 ± 2.19	9.24 ± 3.41	8.31 ± 4.50	7.99 ± 2.69	9.35 ± 2.64	10.90 ± 4.19	11.41 ± 1.48
14-HDoHE : DHA	20.27 ± 5.62	26.70 ± 13.20	32.88 ± 21.15	29.62 ± 10.04	31.78 ± 15.72	25.96 ± 15.37	42.15 ± 15.67
17-HDoHE : DHA	9.80 ± 4.62	9.28 ± 2.44	11.00 ± 5.57	9.83 ± 5.36	12.48 ± 4.56	12.91 ± 8.17	17.28 ± 7.01
Non-enzymatically oxidized lipid metabolites							
F_2-IsoPs : AA	0.00842 ± 0.00182	0.01113 ± 0.00389	0.00901 ± 0.00146	0.00780 ± 0.00139	0.00811 ± 0.00109	0.01120 ± 0.00423	0.01118 ± 0.00488

Table S1(A). Levels of PUFAs and other detectable PUFA metabolites at 6h. Levels of PUFAs were expressed as absolute quantity normalized with the protein content. Levels of PUFA metabolites were expressed as ratio of metabolite to precursor PUFA. All results are shown as mean ± SD (n = 5). Significance tested by one-way ANOVA.

24h	Ctrl	n-TiO_2	b-TiO_2	n-ZnO	b-ZnO	n-Ag	i-Ag
Polyunsaturated fatty acids (PUFAs)							
AA (ng/mg protein)	190.73 ± 39.39	196.90 ± 45.08	225.58 ± 73.56	239.93 ± 57.54	191.43 ± 51.26	192.40 ± 17.45	189.78 ± 34.21
AdA (ng/mg protein)	39.23 ± 13.17	39.94 ± 6.15	38.81 ± 8.83	39.78 ± 3.50	34.08 ± 6.86	33.67 ± 7.56	37.31 ± 10.50
DHA (ng/mg protein)	0.187 ± 0.072	0.128 ± 0.032	0.191 ± 0.096	0.234 ± 0.151	0.244 ± 0.076	0.204 ± 0.059	0.232 ± 0.033
DPA (ng/mg protein)	668.48 ± 320.89	637.38 ± 311.20	701.29 ± 364.75	756.41 ± 268.12	743.60 ± 364.28	829.23 ± 362.44	838.60 ± 211.32
EPA (ng/mg protein)	11361.80 ± 4585.70	14229.71 ± 10682.56	16718.44 ± 10464.01	17637.94 ± 13744.15	14637.73 ± 8091.32	15271.89 ± 8221.45	17264.63 ± 12535.77
Enzymatically oxidized lipid metabolites							
5-HETE : AA	0.00372 ± 0.00088	0.00447 ± 0.00091	0.00461 ± 0.00077	0.00446 ± 0.00165	0.00427 ± 0.00077	0.00660 ± 0.00135**	0.00438 ± 0.00126
8-HETE : AA	0.00319 ± 0.00222	0.00335 ± 0.00167	0.00354 ± 0.00189	0.00315 ± 0.00092	0.00273 ± 0.00095	0.00343 ± 0.00157	0.00291 ± 0.00112
9-HETE : AA	0.00964 ± 0.00671	0.01459 ± 0.00935	0.01957 ± 0.01605	0.01742 ± 0.00632	0.01325 ± 0.00702	0.02175 ± 0.01162	0.01701 ± 0.00590
11-HETE : AA	0.00219 ± 0.00110	0.00251 ± 0.00040	0.00229 ± 0.00157	0.00366 ± 0.00124	0.00266 ± 0.00100	0.00331 ± 0.00093	0.00303 ± 0.00181
12-HETE : AA	0.00365 ± 0.00195	0.00424 ± 0.00258	0.00478 ± 0.00284	0.00601 ± 0.00435	0.00474 ± 0.00299	0.00561 ± 0.00312	0.00485 ± 0.00295
15-HETE : AA	0.00424 ± 0.00273	0.00512 ± 0.00332	0.00537 ± 0.00375	0.00638 ± 0.00416	0.00582 ± 0.00334	0.00712 ± 0.00373	0.00609 ± 0.00326
4-HDoHE : DHA	8.77 ± 2.80	15.07 ± 7.27	12.17 ± 9.03	9.97 ± 4.16	7.74 ± 2.69	10.74 ± 3.57	9.96 ± 4.31
7- HDoHE : DHA	2.46 ± 2.03	4.60 ± 1.91	2.31 ± 0.78	2.48 ± 1.96	2.03 ± 0.76	2.72 ± 0.82	2.43 ± 1.49
8- HDoHE : DHA	12.26 ± 6.85	19.20 ± 14.19	13.34 ± 5.51	18.29 ± 9.22	11.04 ± 7.61	17.75 ± 9.65	14.36 ± 7.44
11- HDoHE : DHA	4.52 ± 2.94	6.03 ± 2.53	5.29 ± 0.77	5.97 ± 2.58	4.77 ± 2.45	7.47 ± 4.22	4.72 ± 2.86
14- HDoHE : DHA	19.30 ± 5.67	29.34 ± 4.97	23.12 ± 6.95	23.18 ± 6.06	12.47 ± 7.73	20.61 ± 9.06	24.15 ± 10.70
17- HDoHE : DHA	6.54 ± 2.90	6.69 ± 0.66	6.98 ± 2.77	10.28 ± 7.02	6.87 ± 6.66	9.88 ± 6.85	8.01 ± 8.45
Non-enzymatically oxidized lipid metabolites							
F_2-IsoPs : AA	0.00897 ± 0.00318	0.01003 ± 0.00364	0.01075 ± 0.00310	0.01279 ± 0.00963	0.01177 ± 0.00441	0.01262 ± 0.00332	0.01134 ± 0.00309

Table S1(B). Levels of PUFAs and other detectable PUFA metabolites at 24h. Levels of PUFAs were expressed as absolute quantity normalized with the protein content. Levels of PUFA metabolites were expressed as ratio of metabolite to precursor PUFA. All results are shown as mean ± SD (n = 5). Significance level **p < 0.01 determined by one-way ANOVA. F2-Isoprostanes (F2-IsoPs)

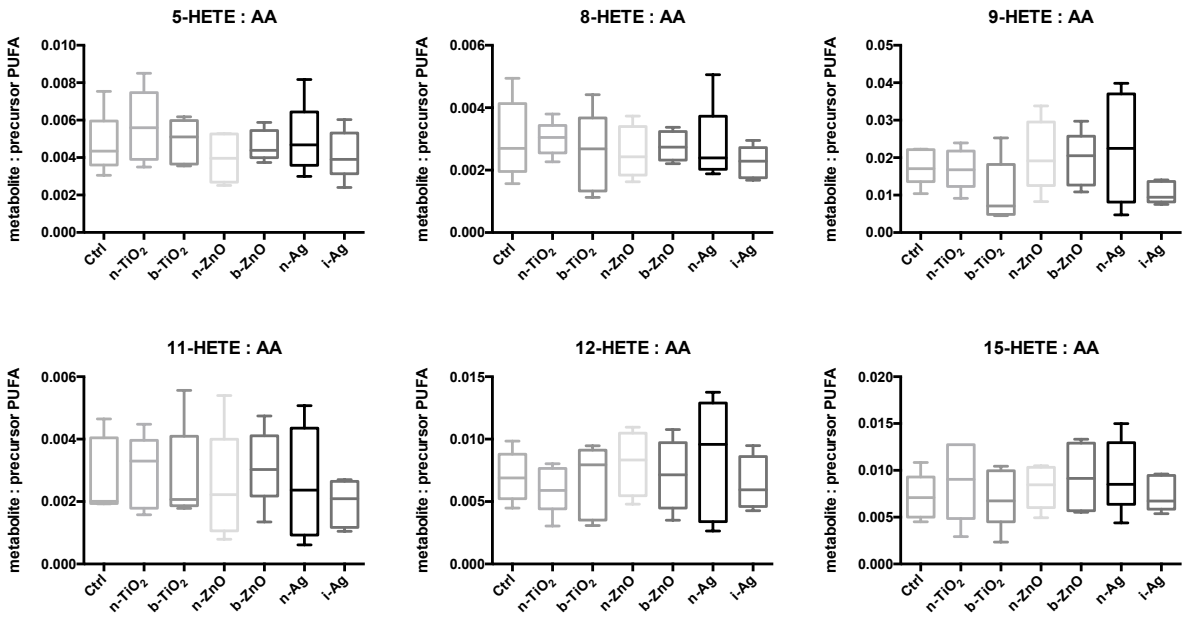

Figure S1. Levels of HETEs at 6h. No significant changes on the AA-to-HETE conversions were observed at 6h across all exposures. Results are expressed as mean ± SD (n = 5).